Biodegradation of metal-based ultra-small nanoparticles: A combined approach using TDA-ICP-MS and CE-ICP-MS

Lucie Labied, Paul Rocchi, Tristan Doussineau, Jérôme Randon, Olivier Tillement, Herve Cottet, François Lux, Agnès Hagège

Biodegradation of metal-based ultra-small nanoparticles: a combined approach using TDA-ICP-MS and CE-ICP-MS

Lucie Labied[a,b], Paul Rocchi[b,c], Tristan Doussineau[c], Jérôme Randon[a], Olivier Tillement[b], Hervé Cottet[e], François Lux[b,d], Agnès Hagège[a],*

[a]Université de Lyon, CNRS, Université Claude Bernard Lyon 1, Institut des Sciences Analytiques, UMR 5280, 69100 Villeurbanne, France, e-mail : agnes.hagege@isa-lyon.fr, phone +(33) 437.423.550
[b]Institut Lumière Matière, Université Claude Bernard Lyon 1, CNRS UMR 5306, 69622 Villeurbanne, France
[c]NH TherAguix S.A.S., 29 Chemin du Vieux Chêne, 38240 Meylan, France
[d]Institut Universitaire de France (IUF), Paris, France
[e]IBMM, University of Montpellier, CNRS, ENSCM, Montpellier, France

Abstract
The knowledge of the fate of metal-containing nanoparticles in biological media in aqueous media is of utmost importance for the future use of these promising theranostic agents for clinical applications. A methodology based on the combination of TDA-ICP-MS and CE-ICP-MS was applied to study the degradation pathway of AGuIX, a phase 2 clinical ultrasmall gadolinium-containing nanoparticle. Nanoparticle size measurements and gadolinium speciation performed in different media (phosphate buffer, urine and serum) demonstrated an accelerated dissolution of AGuIX in serum, without any release of free gadolinium for each medium.

Keywords
Ultrasmall nanoparticles
Gadolinium containing drug
Taylor dispersion analysis
Inductively coupled plasma mass spectrometry
Capillary electrophoresis
Biodegradation

1. Introduction
Nanoparticles are experiencing considerable popularity in the field of nanomedicine, as diagnostic and/or therapeutic agents. Silica-based nanoparticles, either silica or polysiloxane nanoparticles, are particularly attractive due to their good biocompatibility, their low toxicity but also their rich surface functionalization chemistry. As a consequence, studies relating to their potential use as drug carriers, diagnostic, therapeutic or theranostic agents, are increasing, as attested in many publications [1–7] and reviews [8–14].
To meet the safety requirements of national public health agencies, ultra-small nanoparticles (USNPs) with sizes below the glomerular filtration cut-off (< 8 nm) [15] are particularly attractive due to their high renal excretion, minimizing potential health hazards [16,17]. In this context, AGuIX nanoparticle, a gadolinium-containing ultra-small polysiloxane nanoparticle, has been developed, demonstrating very high radiosensitizing effect together with excellent MRI positive contrast properties thanks to the paramagnetic properties of gadolinium [18,19]. This particle has been translated to the clinic for treatment by radiotherapy of brain metastases, cervical cancer, lung cancer and pancreatic cancer.[20,21]
The knowledge of their potential biodegradation in aqueous media is however of utmost importance to promote clinical translation of these nanoparticles [22,23]. A first approach consists in following the size variations of USNPs when in contact with biological media. Dynamic light scattering (DLS) is the most popular technique to determine NP hydrodynamic diameters. However, the measure is strongly biased toward small volume fractions of larger species, which prohibits the determination of USNPs radii in the presence of huge amounts of larger molecules (e.g. proteins in serum) [24,25]. For that reason, methods based on intrinsic properties of the studied USNPs are preferred. Hence, Fluorescence Correlation Spectroscopy was used for the characterization of ultrasmall fluorescent silica nanoparticles [26]. Recently we showed that Taylor Dispersion Analysis (TDA)-ICP-MS is particularly adapted for the measurement of mean hydrodynamic radii of metal-containing particles in biological media [27].
The biodegradability of polysiloxane USNPs in diluted solutions was shown to lead to fragments composed of siloxanes of different compositions [28]. In the case of hybrid nanoparticles containing exogenous metals, biodegradation studies are even more intricate owing to the intrinsic potential toxicity of these metals as free ions in the body [29] and analytical methods should be able to warrant their absence.

As reviewed by Telgmann *et al.*[30], various analytical methods have been developed to determine gadolinium and its complexes in biological and environmental matrices. Capillary zone electrophoresis (CE) is well-adapted to the separation of small molecules, and its hyphenation with ICP-MS has been used for the separation and quantification of numerous metal-containing species. However, only a few studies report its use for the analysis of Gd-containing species. CE coupled with mass spectrometry was used for the analysis of a MRI contrast agent (Gd-BOPTA) in biological fluids like human serum and urine [31]. CE-ICP-MS was applied to separate Gd-DTPA and its potential metabolites. In addition to these types of information, the use of ICP-MS as detection method allows the quantification of the oxidation products [32].
A combination of characterization methods is therefore highly desirable to get useful information in terms of size, charge, and speciation. In the metallic nanoparticle analysis field, recent strategies based on multiple ICP-MS methods have demonstrated their potential. Kruszewska et al. proposed a combination of multiple methods such as CE-ICP-MS, HPLC-ICP-MS and single-particle (sp)-ICP-MS, to better describe the AuNPs fate in biological media by obtaining size of the objects involved and speciation information [33]. Turiel-Fernández *et al.* studied the incorporation of iron oxide nanoparticles cisplatin (IV) nanoconjugates in cells by both HPLC-ICP-MS and single-cell-ICP-MS analysis [34].
We propose to combine TDA-ICP-MS and CE-ICP-MS to study the behavior of ultrasmall metal-containing nanoparticles. Thanks to the introduction of two deconvolution methods for data analysis, TDA-ICP-MS can now be extended to polydisperse samples or mixtures. CE-ICP-MS can then advantageously be exploited for the separation of molecular species. As a proof of principle, this approach will be exemplified hereafter onbiodegradation studies. *In vitro* measurements of the integrity of the nanoparticles (both diameter and polydispersity index), but also the formation of smaller Gd containing species, will be assessed in different media.

2. Materials and methods

2.1. Materials

Tris (Trizma base), NaCl, HCl, EDTA, sodium phosphate mono and dibasic, and hydroxypropylcellulose (average molecular weight 80,000) were purchased from Sigma-Aldrich. Ultrapure HNO_3 65% was obtained from Merck and Gd ICP standard (1000 ppm in HNO_3 1%) from SCP Science.
Serum from human male AB plasma (H4522) and synthetic urine (Surine™ Negative Urine Control) were purchased from Sigma-Aldrich.
AGuIX nanoparticles (gadolinium-chelated polysiloxane nanoparticles) were provided by NH TherAguix as a lyophilized powder and reconstituted at 100 g/L with ultrapure water. Due to their very small size, most of the silicon atoms are located on the surface and involved in at least one siloxane bond.
1,4,7,10-tetraazacyclododecane-1-glutaric anhydride-4,7,10-triacetic acid (DOTAGA), 2,2',2''-(10-(1-carboxy-4-oxo-4-((3-(trihydroxysilyl)propyl)amino)butyl)-1,4,7,10-tetraazacyclododecane-1,4,7-triyl)triacetic acid (APTES-DOTAGA), 2,2',2''-(10-(1-carboxy-4-oxo-4-((3-(1,1,3,3,3-pentahydroxydisiloxaneyl)propyl)amino)butyl)-1,4,7,10-tetraazacyclododecane-1,4,7-triyl)triacetic acid (TEOS-APTES-DOTAGA) and, their Gd complexes were synthesized for helping the identification of gadolinium compounds (see SI).

2.2. Instrumentation

A 7100 capillary electrophoresis system (Agilent) was used for both TDA and CE analyses. Silica capillaries (Photonlines, length 70 cm, 75 µm i.d., 375 µm o.d.) were thermally coated with hydroxypropylcellulose using the method described by Shen *et al.* [35] and rinsed at 1 bar with the running buffer for 10 min prior to first use.
Detection of gadolinium was enabled by hyphenation with a Nexion 300X ICP-MS (Perkin Elmer). Gd signal was monitored at m/z 158, with a dwell time of 500 ms. Operating conditions used for the ICP-MS were: nebulizer gas flow rate, 1.09 L/min; plasma gas flow rate, 18 L/ min; auxiliary gas flow rate, 1.2 L/min; radiofrequency power, 1600 W for the plasma. All other parameters were tuned to maximize the Gd signal.
3D-CE Chemstation software version B.04.03 (Agilent) was used to control the CE system and Syngistix software version 2.3 was used to both control the ICP-MS and acquire the Gd signal.

2.3. Sample preparation for biodegradation experiments

0.5 g/L AGuIX solutions were prepared by dilution in different media. These media were either aqueous buffers, i.e. Tris buffer (Tris 10 mM, NaCl 100 mM, pH 7.4) and sodium phosphate buffer (phosphate 10 mM, NaCl 100 mM), or serum, which was used without any treatment or dilution. The AGuIX solutions were kept at room temperature without stirring and aliquots were collected and injected at different times either for size measurement or for Gd speciation.

2.4. Size measurements by TDA-ICP-MS

The interface used for TDA consisted in a T-connector where the capillary outlet was inserted through and then connected to the ICP-MS. A sheath liquid (HNO_3 1 mM) was added to the junction in order to compensate for the self-aspiration of the nebulizer and to allow quantification without matrix matching as described in [27]. TDA experiments were conducted with an applied mobilization pressure of 50 mbar. Aliquots collected during biodegradation were injected at 20 mbar for 3 s. The mobilization media used were identical to the used biodegradation media, i. e. either aqueous buffers (Tris 10 mM NaCl 150 mM, pH 7.4 or sodium phosphate 10 mM, NaCl 150 mM, pH 7.4) or biological media (human blood serum or synthetic urine). Between runs, the capillaries were flushed at 1 bar for 2 min with the mobilization medium.

2.5. Gd speciation by CE-ICP-MS

For CE-ICP-MS, the capillary outlet was inserted through a cross-connector, as a fourth inlet was necessary for the electrode. It was then connected to the nebulizer. A platinum electrode and a sheath liquid (sodium phosphate 5 mM, pH 7) were added to the cross-connector in order to close the electrical circuit and compensate for the self-aspiration, as described elsewhere [36]. CE analyses were carried out using sodium phosphate 10 mM pH 7 as background electrolyte (BGE). The samples from AGuIX biodegradation were injected at 50 mbar for 3 s, and the separation was conducted under a voltage of -25 kV assisted by an applied pressure of 10 mbar. Between runs, the capillaries were flushed at 1 bar for 2 min with BGE.

3. Results and discussion

3.1. Assessing different populations sizes and polydispersity index by TDA-ICP-MS analyses

TDA-ICP-MS has been successfully applied to determine an average size of the AGuIX USNPs [27]. However, a monomodal description of the AGuIX USNP is not sufficient to fully describe the degradation process that may occur in different media. Assuming two differently sized populations in the sample, (e.g. a nano-object and small molecules), the taylorgram obtained by Taylor Dispersion Analysis can be assimilated to the sum of two Gaussians signals:

$$S(t) = \sum_{i=1}^{2} \frac{A_i}{\sigma_i \sqrt{2\pi}} \exp\left(-\frac{(t-t_0)^2}{2\sigma_i^2}\right) \quad (1)$$

where t_0 is the peak residence time, A_i and σ_i are the area under the curve and temporal variance associated with Gd-containing species i (i = 1 or 2). Comparison between monomodal and bimodal fitting is given in SI (figure S1).

Since NPs' size directly influences the transport and excretion of nanoparticles, determination of a mean diameter is not sufficient and should be complemented by the determination of the entire distribution.

The constrained regularized linear inversion (CRLI) method, developed by Cipelletti *et al.* [37], seems to allow this determination. Instead of making any assumption about the number of populations present in the sample, the taylorgram is fitted following an adaptation of the CONTIN algorithm, already well established in DLS data treatment, to TDA data. A representative taylorgram and corresponding bimodal and CRLI deconvolutions of AGuIX diluted at 0.5 g/L in Tris NaCl buffer are given in figure 1. Corresponding results for hydrodynamic diameters and Gd repartition are given in table 1. The given error bars correspond to results obtained over 5 repetitions, at 95% confidence interval. The mean diameter value given for CRLI fitting results is the weighted average of the NP peak of the distribution.

Table 1: Hydrodynamic diameters and Gd repartition from TDA experiments

	Fragment hydrodynamic diameter (nm)	**USNP hydrodynamic diameter (nm)**	**Gd proportion in USNP (%)**
Bimodal deconvolution	1.2 ± 0.7 nm	5.6 ± 0.2 nm	87 ± 5 %
CRLI	1.8 ± 1.6 nm	5.4 ± 0.2 nm	91 ± 7 %

From both deconvolutions methods (bimodal deconvolution and CRLI), it can be seen that gadolinium is distributed into two populations. The main population corresponds to USNPs. Obtained USNP diameters and Gd proportions are very similar for the two data treatment processes. The second population corresponds to Gd species of smaller size. Both data processes give a mean hydrodynamic diameter in reasonable agreement

(1.2 and 1.8 nm for bimodal and CRLI deconvolution respectively), displaying however higher uncertainty. Such population is consistent with the presence of small Gd species that may correspond to either USNPs fragments or unreacted compounds.
Here, by applying CRLI deconvolution method, TDA-ICP-MS demonstrated its added-value in comparison with DLS routine experiments, allowing discrimination of sub-populations having mean diameters differences of only a few nanometers.
The size distribution obtained by CRLI can give information regarding the polydispersity of the USNP, and confirms that even the bigger particles stay below the renal elimination cut-off.

3.2. Following the Gd-containing USNP biodegradation by TDA-ICP-MS

AGuIX biodegradation has been monitored in aqueous buffer and human blood serum by TDA-ICP-MS. For that purpose, the nanoparticle was diluted at 0.5 g/L in each studied medium, namely NaCl solutions at physiological pH in either Tris or phosphate buffer, or human blood serum, and left to incubate at room temperature, without stirring. TDA-ICP-MS, using the incubation medium as buffer, has been performed at regular intervals in order to monitor the biodegradation rate of the particle and the impact of the medium. Resulting hydrodynamic diameters and Gd proportions in the sample obtained by bimodal fitting, as well as their evolution with incubation time (t_{inc}), are given in figure 2.

At t_{inc}=0, the hydrodynamic size of the AGuIX UNSPs is similar in both types of media, illustrating their colloidal stability. Moreover, an absence of interactions with proteins in serum was noticed, as already reported in others papers [27,38,39].
Soon after dilution, a process of biodegradation occurs as asserted by the USNP size decrease. This process seems to be medium-dependent (Figure 2, and c). In both Tris and sodium phosphate buffers, the USNP size decreases slightly in 6 h while the USNP Gd content slowly decreases from 85% to 60% in the same time frame (Figure 2b). Similarly, AGuIX USNP biodegradation was monitored in synthetic urine (see SI, figure S2). The obtained biodegradation profile was similar to the results in aqueous buffers.

In human blood serum, a more important biodegradation was observed. USNP size first decreases from 6 to 3.6 nm in 10 hours, accompanied by a very significant linear decrease of the gadolinium proportion corresponding to the particle sub-population (Figure 2d). After 10 h incubation, Gd is mainly involved in smaller complexes. At this stage, only around 10% of the detected Gd is part of particle sub-population whose mean diameter seems to be bigger than the initial USNP, as shown by the sharp increase of its respective size after 10 h. However, the formation of a protein corona with such slow kinetics seems very unlikely. This apparent increase in diameter could be linked to the uncertainty of the bimodal fitting for larger objects in small proportions. Since the height of the peak is inversely proportional to the diameter of the solute, the size-related information can be skewed by the signal noise at the bottom of the peak and can lead to a slight overestimation of the measured diameter. Simulations of taylorgrams realized for a sample composed of 90% small molecules and 10% 8 nm USNPs, with different levels of noise showed that bimodal fitting on a noisy signal often overestimates the size of the nanoparticle, but accurately estimates the proportions (see SI, figure S3).
These results might indicate a surface erosion of the nanoparticle leading to a release of the Gd-containing moieties that occurs step-by-step and may be attributed to a dissolution of the polysiloxane matrix by hydrolysis of the Si−O−Si bonds.
This accelerated biodegradation in biological media was already observed by S.-A. Yang et al. [40] who found that amino-rich compounds in cell culture medium as well as blood are particularly involved in the degradation of silica layers by medium components.
In order to monitor a possible change in polydispersity of the USNP, CRLI fitting was performed on the taylorgrams of AGuIX in serum, and are given in SI (figure S4). The proportions and diameters for both populations follow the trend obtained by bimodal fitting. Moreover, the NP size stays below the cut-off size for renal elimination up to 9 hours incubation.
This biodegradation trend is in perfect agreement with relaxometry as well, as shown in SI (figure S5). This method is sensitive to the size of Gd-containing species, and was used in previous biodegradation studies of Gd-based USNP [38,41]. Higher relaxivity values are observed for large objects due to decrease of rotational correlation time, while smaller values are indicative of molecular species. At the end of the kinetic study in serum, r_1 is close to 5 $mM^{-1}.s^{-1}$ at 1.4 T, similar to r_1 of commercial molecular agents measured at this magnetic field [42].

3.3. Following the variation of Gd speciation by CE-ICP-MS

TDA experiments have shown the existence of small molecules together with the USNP just after dilution of AGuIX, but are not able to differentiate all the small molecules present in the sample. Hence, a CE-ICP-MS separation has been developed to assess the Gd-containing species in AGuIX USNP solutions.
CE separation of the nanoparticle from its byproducts has first been achieved in phosphate buffer at pH 7, on an HPC-coated fused silica capillary. Then, as for TDA, AGuIX USNPs were diluted at 0.5 g/L either in phosphate buffer or human blood serum.
The sample was then injected at regular intervals, and the CE separation was followed by ICP-MS. EDTA was previously added to AGuIX diluted in serum to avoid Gd precipitation at pH 7 and free Gd was then detected as Gd-EDTA complex. Despite careful calibration of pressure compensation through the CE-ICP-MS interface described in section *2.5*, good reproducibility of migration times was challenging. The obtained electropherograms were converted into mobilograms in order to compensate for the small pressure variations, and intensities corrected by multiplying the acquired signal by the square of the migration time, according to Chamieh et al.[43]. The resulting mobilograms are given in figure 3. Original electropherograms are available in SI (figure S6).

CE-ICP-MS experiments confirm the presence of both NPs and smaller species containing Gd, the mobilograms exhibiting 6 main Gd-containing peaks. The mobilograms of the USNP diluted in human blood serum (Figure 3c) are similar to those obtained after dilution in phosphate buffer (Fig 3a), although significant peak broadening is observed. This can be attributed to the higher viscosity and salinity of the injected serum plug that enhances dispersion, the electrophoretic mobilities in the injection plug being lower than those in the BGE.
The USNP peak (peak 6) is large, which may suggest a relatively wide surface charge/size ratio disparity. Moreover, the electrophoretic mobility of the USNP seems to be strongly affected by biodegradation, especially in human blood serum where peak 6 fully merges with peak 5 after 7h (see SI, figure S7).

During biodegradation, the first 4 peaks remain constant in their proportions over the time, while peak 5 increases steadily and significantly after dilution (Figure 3d). The total Gd content was found to be constant over all CE analyses. The USNP proportions determined from the mobilograms are in good agreement with those obtained by bimodal fitting of taylorgrams.
Attempts to identify other Gd compounds (Peaks 1-5) were performed by comparison with in-lab synthesized suspected degradation products or byproducts. Corresponding mobilograms of the synthesized compounds are provided in SI (figure S8). Peak 1 was attributed to DOTAGA-Gd chelates, while peaks 4 and 5 were found to be present in both APTES-DOTAGA-Gd and TEOS + APTES-DOTAGA-Gd mixtures. Peaks 2 and 3 remain unknown until now.
It can then be assumed that biodegradation occurs through the hydrolysis of Si-O-Si bonds holding DOTAGA-Gd complexes grafted on the surface of the nanoparticle, and APTES-DOTAGA-Gd species were likely to be released. As a result, the following degradation scheme can be proposed (Figure 4).

3.4. Detection of free Gadolinium content in AGuIX

It seems that the only Gd-containing product resulting from AGuIX degradation is APTES-DOTAGA-Gd.
However, a special concern regarding AGuIX USNPs (as well as other gadolinium-based therapeutic drugs) is the potential release of free gadolinium in the organism, which has been proven to be harmful for patients [29].
For a safe use of these particles, free gadolinium release must be avoided. In the CE-ICP-MS configuration used for these analyses, the detection limit was found to be 1.5 µM (data not shown). In order to ascertain a free gadolinium content in the samples as low as possible, the biodegradation process was monitored at a concentration of 5 g/L.

AGuIX was diluted at 5 g/L in human blood serum. In order to detect potential free Gd release, EDTA was added prior to CE analysis. In parallel, a second sample was spiked with EDTA-Gd. Both samples were monitored at 1h, 5h and 24h incubation time by CE-ICP-MS, and resulting mobilograms are given in figure 5. The EDTA-Gd peak was only detected in the Gd spiked AGuIX sample, and was absent from the non-spiked sample, indicating that free gadolinium is not released above the method detection limit during AGuIX biodegradation in serum.

4. Conclusion

The biodegradation of a Gd based USNP was followed with two methods, TDA-ICP-MS and CE-ICP-MS. Bimodal gaussian fitting of TDA data allows the determination of size and relative proportions of two Gd-containing

populations of size below 6 nm, in less than 20 minutes. CRLI approach allows to get insight about the structure of the entire size distribution, and therefore, valuable information on sample polydispersity. The ease of use of this method allowed a close monitoring of USNPs biodegradation in a wide range of media, from aqueous buffers to highly complex matrices such as blood serum. The results of TDA-ICP-MS for particle biodegradation were found to be in agreement with those obtained from CE-ICP-MS separation. CE-ICP-MS has then been used to monitor the Gd-containing biodegradation products and appeared to be a useful complementary tool, as these compounds can be fully separated. Indeed, this hyphenation demonstrated that the AGuIX biodegradation main product is likely APTES-DOTAGA-Gd. Moreover, no evidence of free Gd release upon biodegradation was provided by the CE-ICP-MS experiments.
Hence, it should be a promising approach for investigations of metal-containing USNPs behavior in biologically-relevant conditions.

5. Acknowledgement

This work is part of the Analytaguix project and has been supported by a French Government Grant managed by the French National Research Agency (ANR-18-CE17-0025-02).

REFERENCES

[1] Z. Qin, B. Chen, Y. Mao, C. Shi, Y. Li, X. Huang, F. Yang, N. Gu, Achieving Ultrasmall Prussian Blue Nanoparticles as High-Performance Biomedical Agents with Multifunctions, ACS Appl. Mater. Interfaces. 12 (2020) 57382–57390. https://doi.org/10.1021/acsami.0c18357.

[2] M. Cui, C. Wiraja, L.W. Qi, S.C.W. Ting, D. Jana, M. Zheng, X. Hu, C. Xu, One-step synthesis of amine-coated ultra-small mesoporous silica nanoparticles, Nano Res. 13 (2020) 1592–1596. https://doi.org/10.1007/s12274-020-2775-z.

[3] W. Wen, L. Wu, Y. Chen, X. Qi, J. Cao, X. Zhang, W. Ma, Y. Ge, S. Shen, Ultra-small Fe3O4 nanoparticles for nuclei targeting drug delivery and photothermal therapy, J. Drug Deliv. Sci. Technol. 58 (2020) 101782. https://doi.org/10.1016/j.jddst.2020.101782.

[4] F. Chen, K. Ma, M. Benezra, L. Zhang, S.M. Cheal, E. Phillips, B. Yoo, M. Pauliah, M. Overholtzer, P. Zanzonico, S. Sequeira, M. Gonen, T. Quinn, U. Wiesner, M.S. Bradbury, Cancer-Targeting Ultrasmall Silica Nanoparticles for Clinical Translation: Physicochemical Structure and Biological Property Correlations, Chem. Mater. 29 (2017) 8766–8779. https://doi.org/10.1021/acs.chemmater.7b03033.

[5] K. Wey, M. Epple, Ultrasmall gold and silver/gold nanoparticles (2 nm) as autofluorescent labels for poly(D,L-lactide-co-glycolide) nanoparticles (140 nm), J. Mater. Sci. Mater. Med. 31 (2020) 117. https://doi.org/10.1007/s10856-020-06449-8.

[6] D.-Y. Zhang, H. Liu, T. He, M.R. Younis, T. Tu, C. Yang, J. Zhang, J. Lin, J. Qu, P. Huang, Biodegradable Self-Assembled Ultrasmall Nanodots as Reactive Oxygen/Nitrogen Species Scavengers for Theranostic Application in Acute Kidney Injury, Small. n/a (n.d.) 2005113. https://doi.org/10.1002/smll.202005113.

[7] J.A. Erstling, J.A. Hinckley, N. Bag, J. Hersh, G.B. Feuer, R. Lee, H.F. Malarkey, F. Yu, K. Ma, B.A. Baird, U.B. Wiesner, Ultrasmall, Bright, and Photostable Fluorescent Core–Shell Aluminosilicate Nanoparticles for Live-Cell Optical Super-Resolution Microscopy, Adv. Mater. n/a (n.d.) 2006829. https://doi.org/10.1002/adma.202006829.

[8] J. Xu, C. Peng, M. Yu, J. Zheng, Renal clearable noble metal nanoparticles: photoluminescence, elimination, and biomedical applications, WIREs Nanomedicine Nanobiotechnology. 9 (2017) e1453. https://doi.org/10.1002/wnan.1453.

[9] B.H. Kim, M.J. Hackett, J. Park, T. Hyeon, Synthesis, Characterization, and Application of Ultrasmall Nanoparticles, Chem. Mater. 26 (2014) 59–71. https://doi.org/10.1021/cm402225z.

[10] Y. Zhang, C. Zhang, C. Xu, X. Wang, C. Liu, G.I.N. Waterhouse, Y. Wang, H. Yin, Ultrasmall Au nanoclusters for biomedical and biosensing applications: A mini-review, Talanta. 200 (2019) 432–442. https://doi.org/10.1016/j.talanta.2019.03.068.

[11] M. Fan, Y. Han, S. Gao, H. Yan, L. Cao, Z. Li, X.-J. Liang, J. Zhang, Ultrasmall gold nanoparticles in cancer diagnosis and therapy, Theranostics. 10 (2020) 4944–4957. https://doi.org/10.7150/thno.42471.

[12] K. Zarschler, L. Rocks, N. Licciardello, L. Boselli, E. Polo, K.P. Garcia, L. De Cola, H. Stephan, K.A. Dawson, Ultrasmall inorganic nanoparticles: State-of-the-art and perspectives for biomedical applications, Nanomedicine Nanotechnol. Biol. Med. 12 (2016) 1663–1701. https://doi.org/10.1016/j.nano.2016.02.019.

[13] C. Song, W. Sun, Y. Xiao, X. Shi, Ultrasmall iron oxide nanoparticles: synthesis, surface modification, assembly, and biomedical applications, Drug Discov. Today. 24 (2019) 835–844. https://doi.org/10.1016/j.drudis.2019.01.001.

[14] X. Jiang, B. Du, Y. Huang, J. Zheng, Ultrasmall noble metal nanoparticles: Breakthroughs and biomedical implications, Nano Today. 21 (2018) 106–125. https://doi.org/10.1016/j.nantod.2018.06.006.

[15] B. Du, M. Yu, J. Zheng, Transport and interactions of nanoparticles in the kidneys, Nat. Rev. Mater. 3 (2018) 358–374. https://doi.org/10.1038/s41578-018-0038-3.

[16] M. Yu, J. Zheng, Clearance Pathways and Tumor Targeting of Imaging Nanoparticles, ACS Nano. 9 (2015) 6655–6674. https://doi.org/10.1021/acsnano.5b01320.

[17] M. Longmire, P.L. Choyke, H. Kobayashi, Clearance properties of nano-sized particles and molecules as imaging agents: considerations and caveats, Nanomed. 3 (2008) 703–717. https://doi.org/10.2217/17435889.3.5.703.
[18] F. Lux, V.L. Tran, E. Thomas, S. Dufort, F. Rossetti, M. Martini, C. Truillet, T. Doussineau, G. Bort, F. Denat, F. Boschetti, G. Angelovski, A. Detappe, Y. Crémillieux, N. Mignet, B.-T. Doan, B. Larrat, S. Meriaux, E. Barbier, S. Roux, P. Fries, A. Müller, M.-C. Abadjian, C. Anderson, E. Canet-Soulas, P. Bouziotis, M. Barberi-Heyob, C. Frochot, C. Verry, J. Balosso, M. Evans, J. Sidi-Boumedine, M. Janier, K. Butterworth, S. McMahon, K. Prise, M.-T. Aloy, D. Ardail, C. Rodriguez-Lafrasse, E. Porcel, S. Lacombe, R. Berbeco, A. Allouch, J.-L. Perfettini, C. Chargari, E. Deutsch, G.L. Duc, AGuIX® from bench to bedside—Transfer of an ultrasmall theranostic gadolinium-based nanoparticle to clinical medicine, Br J Radiol. (n.d.) 19.
[19] G. Bort, F. Lux, S. Dufort, Y. Crémillieux, C. Verry, O. Tillement, EPR-mediated tumor targeting using ultrasmall-hybrid nanoparticles: From animal to human with theranostic AGuIX nanoparticles, Theranostics. 10 (2020) 1319–1331. https://doi.org/10.7150/thno.37543.
[20] C. Verry, S. Dufort, J. Villa, M. Gavard, C. Iriart, S. Grand, J. Charles, B. Chovelon, J.-L. Cracowski, J.-L. Quesada, C. Mendoza, L. Sancey, A. Lehmann, F. Jover, J.-Y. Giraud, F. Lux, Y. Crémillieux, S. McMahon, P.J. Pauwels, D. Cagney, R. Berbeco, A. Aizer, E. Deutsch, M. Loeffler, G. Le Duc, O. Tillement, J. Balosso, Theranostic AGuIX nanoparticles as radiosensitizer: A phase I, dose-escalation study in patients with multiple brain metastases (NANO-RAD trial), Radiother. Oncol. 160 (2021) 159–165. https://doi.org/10.1016/j.radonc.2021.04.021.
[21] C. Verry, S. Dufort, B. Lemasson, S. Grand, J. Pietras, I. Troprès, Y. Crémillieux, F. Lux, S. Mériaux, B. Larrat, J. Balosso, G.L. Duc, E.L. Barbier, O. Tillement, Targeting brain metastases with ultrasmall theranostic nanoparticles, a first-in-human trial from an MRI perspective, Sci. Adv. 6 (2020) eaay5279. https://doi.org/10.1126/sciadv.aay5279.
[22] S. Roy, Z. Liu, X. Sun, M. Gharib, H. Yan, Y. Huang, S. Megahed, M. Schnabel, D. Zhu, N. Feliu, I. Chakraborty, C. Sanchez-Cano, A.M. Alkilany, W.J. Parak, Assembly and Degradation of Inorganic Nanoparticles in Biological Environments, Bioconjug. Chem. 30 (2019) 2751–2762. https://doi.org/10.1021/acs.bioconjchem.9b00645.
[23] A. Ahamed, L. Liang, M.Y. Lee, J. Bobacka, G. Lisak, Too small to matter? Physicochemical transformation and toxicity of engineered nTiO2, nSiO2, nZnO, carbon nanotubes, and nAg, J. Hazard. Mater. 404 (2021) 124107. https://doi.org/10.1016/j.jhazmat.2020.124107.
[24] A. Hawe, W.L. Hulse, W. Jiskoot, R.T. Forbes, Taylor Dispersion Analysis Compared to Dynamic Light Scattering for the Size Analysis of Therapeutic Peptides and Proteins and Their Aggregates, Pharm. Res. 28 (2011) 2302–2310. https://doi.org/10.1007/s11095-011-0460-3.
[25] E. Tomaszewska, K. Soliwoda, K. Kadziola, B. Tkacz-Szczesna, G. Celichowski, M. Cichomski, W. Szmaja, J. Grobelny, Detection Limits of DLS and UV-Vis Spectroscopy in Characterization of Polydisperse Nanoparticles Colloids, J. Nanomater. 2013 (2013) 1–10. https://doi.org/10.1155/2013/313081.
[26] K. Ma, H. Sai, U. Wiesner, Ultrasmall Sub-10 nm Near-Infrared Fluorescent Mesoporous Silica Nanoparticles, J. Am. Chem. Soc. 134 (2012) 13180–13183. https://doi.org/10.1021/ja3049783.
[27] L. Labied, P. Rocchi, T. Doussineau, J. Randon, O. Tillement, F. Lux, A. Hagège, Taylor Dispersion Analysis Coupled to Inductively Coupled Plasma-Mass Spectrometry for Ultrasmall Nanoparticle Size Measurement: From Drug Product to Biological Media Studies, Anal. Chem. 93 (2021) 1254–1259. https://doi.org/10.1021/acs.analchem.0c03988.
[28] C. Truillet, F. Lux, O. Tillement, P. Dugourd, R. Antoine, Coupling of HPLC with Electrospray Ionization Mass Spectrometry for Studying the Aging of Ultrasmall Multifunctional Gadolinium-Based Silica Nanoparticles, Anal. Chem. 85 (2013) 10440–10447. https://doi.org/10.1021/ac402429p.
[29] T. Grobner, Gadolinium--a specific trigger for the development of nephrogenic fibrosing dermopathy and nephrogenic systemic fibrosis?, Nephrol. Dial. Transplant. Off. Publ. Eur. Dial. Transpl. Assoc. - Eur. Ren. Assoc. 21 (2006) 1104–1108. https://doi.org/10.1093/ndt/gfk062.
[30] L. Telgmann, M. Sperling, U. Karst, Determination of gadolinium-based MRI contrast agents in biological and environmental samples: A review, Anal. Chim. Acta. 764 (2013) 1–16. https://doi.org/10.1016/j.aca.2012.12.007.
[31] C. Campa, M. Rossi, A. Flamigni, E. Baiutti, A. Coslovi, L. Calabi, Analysis of gadobenate dimeglumine by capillary zone electrophoresis coupled with electrospray-mass spectrometry, ELECTROPHORESIS. 26 (2005) 1533–1540. https://doi.org/10.1002/elps.200410111.
[32] L. Telgmann, H. Faber, S. Jahn, D. Melles, H. Simon, M. Sperling, U. Karst, Identification and quantification of potential metabolites of Gd-based contrast agents by electrochemistry/separations/mass spectrometry, J. Chromatogr. A. 1240 (2012) 147–155. https://doi.org/10.1016/j.chroma.2012.03.088.
[33] J. Kruszewska, D. Kulpińska, I. Grabowska-Jadach, M. Matczuk, Joint forces of direct, single particle, CE– and HPLC–inductively coupled plasma mass spectrometry techniques for the examination of gold nanoparticle accumulation, distribution and changes inside human cells†, Metallomics. 12 (2020) 408–415. https://doi.org/10.1039/c9mt00309f.
[34] D. Turiel-Fernández, L. Gutiérrez-Romero, M. Corte-Rodriguez, J. Bettmer, M. Montes-Bayón, Ultrasmall iron oxide nanoparticles cisplatin (IV) prodrug nanoconjugate: ICP-MS based strategies to evaluate the formation and drug delivery capabilities in single cells, Anal. Chim. Acta. 1159 (2021) 338356. https://doi.org/10.1016/j.aca.2021.338356.
[35] Y. Shen, S.J. Berger, G.A. Anderson, R.D. Smith, High-efficiency capillary isoelectric focusing of peptides, Anal. Chem. 72 (2000) 2154–2159. https://doi.org/10.1021/ac991367t.
[36] F. Varenne, M. Bourdillon, M. Meyer, Y. Lin, M. Brellier, R. Baati, L.J. Charbonnière, A. Wagner, E. Doris, F. Taran, A. Hagège, Capillary electrophoresis-inductively coupled plasma-mass spectrometry hyphenation for the determination

at the nanogram scale of metal affinities and binding constants of phosphorylated ligands, J. Chromatogr. A. 1229 (2012) 280–287. https://doi.org/10.1016/j.chroma.2012.01.066.
[37] L. Cipelletti, J.-P. Biron, M. Martin, H. Cottet, Measuring Arbitrary Diffusion Coefficient Distributions of Nano-Objects by Taylor Dispersion Analysis, Anal. Chem. 87 (2015) 8489–8496. https://doi.org/10.1021/acs.analchem.5b02053.
[38] M. Dentamaro, F. Lux, L.V. Elst, N. Dauguet, S. Montante, A. Moussaron, C. Burtea, R.N. Muller, O. Tillement, S. Laurent, Chemical and in vitro characterizations of a promising bimodal AGuIX probe able to target apoptotic cells for applications in MRI and optical imaging, Contrast Media Mol. Imaging. 11 (2016) 381–395. https://doi.org/10.1002/cmmi.1702.
[39] X. Yang, M. Bolsa-Ferruz, L. Marichal, E. Porcel, D. Salado-Leza, F. Lux, O. Tillement, J.-P. Renault, S. Pin, F. Wien, S. Lacombe, Human Serum Albumin in the Presence of AGuIX Nanoagents: Structure Stabilisation without Direct Interaction, Int. J. Mol. Sci. 21 (2020). https://doi.org/10.3390/ijms21134673.
[40] S.A. Yang, S. Choi, S.M. Jeon, J. Yu, Silica nanoparticle stability in biological media revisited, Scientific Reports, 8 (2018) 8. https://doi.org/10.1038/s41598-017-18502-8
[41] G. Le Duc, S. Roux, A. Paruta-Tuarez, S. Dufort, E. Brauer, A. Marais, C. Truillet, L. Sancey, P. Perriat, F. Lux, O. Tillement, Advantages of gadolinium based ultrasmall nanoparticles vs molecular gadolinium chelates for radiotherapy guided by MRI for glioma treatment, Cancer Nanotechnol. 5 (2014) 4. https://doi.org/10.1186/s12645-014-0004-8.
[42] P. Caravan, J.J. Ellison, T.J. McMurry, R.B. Lauffer, Gadolinium(III) Chelates as MRI Contrast Agents: Structure, Dynamics, and Applications, Chem. Rev. 99 (1999) 2293–2352. https://doi.org/10.1021/cr980440x.
[43] J. Chamieh, M. Martin, H. Cottet, Quantitative Analysis in Capillary Electrophoresis: Transformation of Raw Electropherograms into Continuous Distributions, Anal. Chem. 87 (2015) 1050–1057. https://doi.org/10.1021/ac503789s.

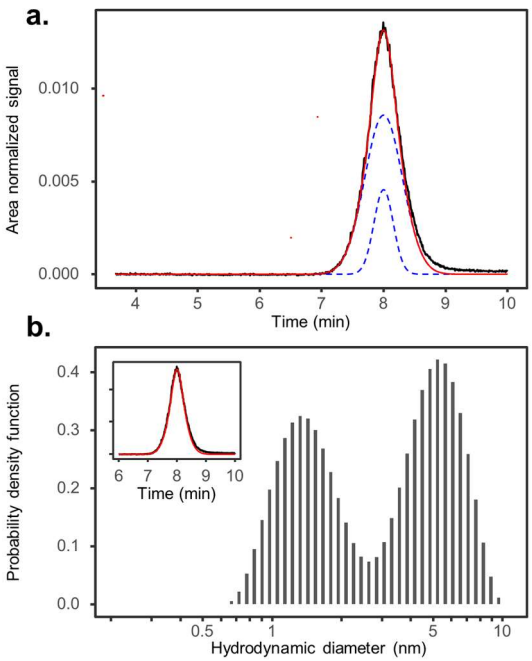

Figure 1. Representative taylorgram and corresponding fit. a) Bimodal fitting: the signal (black line) was fitted with the sum (red line) of two gaussian curves (blue dashed lines). b) CRLI fit: the obtained distribution for hydrodynamic diameters is shown, as well as the signal (black line) and the fitted curve (red line) (insert).Experimental conditions: HPC capillary (75 µm i.d., length 70 cm); buffer Tris 10 mM NaCl 150 mM, pH 7.4; injection 20 mbar 3 s; applied pressure 50 mbar; detection at m/z = 158, dwell time 500 ms.

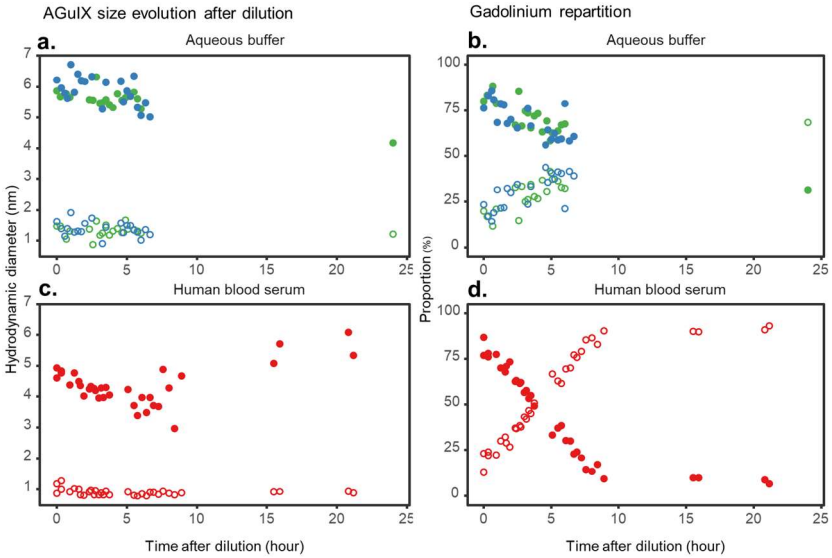

Figure 2. Size evolution (a and c) and Gd repartition (b and d) on either small fragments (empty circles) or USNP (filled circles) for AGuIX USNP after dilution at 0.5 g/L in sodium phosphate 10 mM, NaCl 125 mM, pH 7.0 buffer (in blue), tris 10 mM NaCl 150 mM pH 7.4 (in green) and human blood serum (in red), followed by TDA-ICP-MS. Experimental conditions: HPC capillary (75 µm i.d., length 70 cm) filled with the same dilution medium as the sample (human blood serum, tris or phosphate buffer); injection 20 mbar 3 s; applied pressure 50 mbar; detection at m/z = 158, dwell time 500 ms.

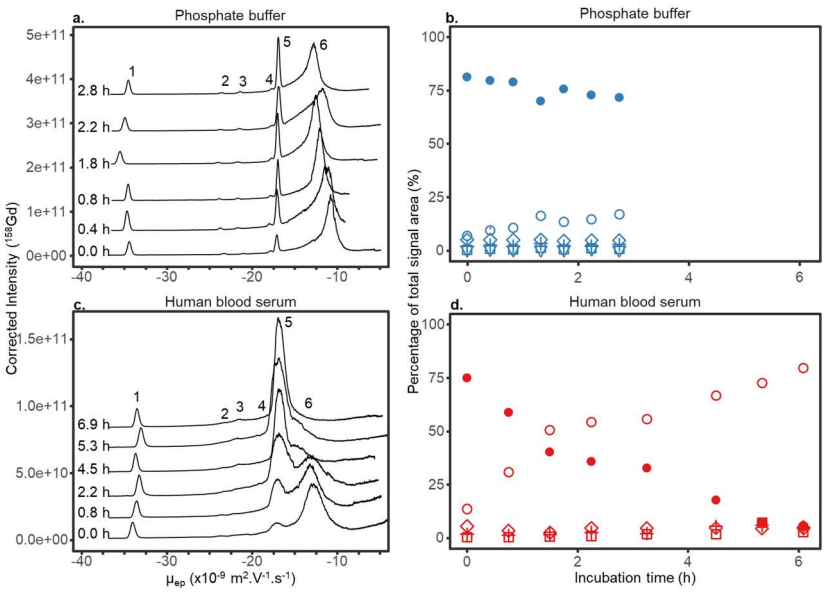

Figure 3 : Mobilograms of AGuIX diluted at 0.5 g/L in the phosphate electrolyte (a) and human blood serum (c), obtained by CE-ICP-MS after different incubation times at room temperature. Proportion of Gd in each of the identified peaks for sodium phosphate buffer (b) and human blood serum (d): nanoparticle (peak 6, filled circles), APTES-DOTAGA-Gd (peak 5, empty circles), DOTAGA-Gd (peak 1, empty diamonds), and the unknown species (peak 2, empty inverted triangle; peak 3, empty squares; peak 4, plus sign). Experimental conditions: HPC capillary (75 µm i.d., length 70 cm); BGE sodium phosphate 10 mM, pH 7.0; injection 50 mbar 3 s; separation -25 kV, 10 mbar; detection at m/z = 158, dwell time 500 ms. Intensities were corrected by multiplying the acquired signal by the square of the migration time, according to Chamieh et al.[43]

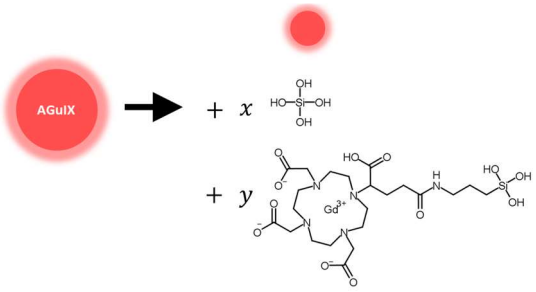

Figure 4: Proposed scheme for AGuIX biodegradation process

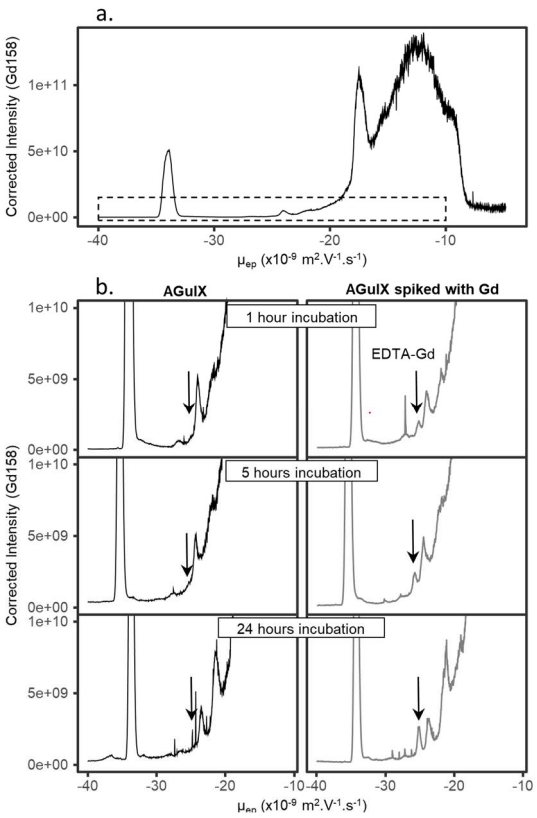

Figure 5: (a) Mobilogram of AGuIX diluted at 5 g/L in a solution of 90% human blood serum + EDTA 3.8 mM after 1 hour incubation time. The dashed box indicates the focus on the EDTA-Gd peak migration region, given in (b) for AGuIX-EDTA (left, black lines) and for the same sample spiked with Gd 6.4 µM (right, grey lines) for 3 incubation times. In both cases, the EDTA-Gd peak mobility is designated by the arrow. Experimental conditions: HPC capillary (75 µm i.d., length 70 cm); BGE sodium phosphate 10 mM, pH 7.0; injection 50 mbar 3 s; separation -25 kV, 10 mbar; detection at m/z = 158, dwell time 500 ms. Intensities were corrected by multiplying the acquired signal by the square of the migration time, according to Chamieh et al[43].